

Optical readout of hydrogen storage in films of Au and Pd

YOSHIAKI NISHIJIMA,^{1,*} SHOGO SHIMIZU,¹ KEISUKE KURIHARA,¹
YOSHIKAZU HASHIMOTO,¹ HAJIME TAKAHASHI,² ARMANDAS
BALČYTIS,^{3,4} GEDIMINAS SENIUTINAS,^{3,5} SHINJI OKAZAKI,² JURGA
JUODKAZYTĖ,⁴ TAKESHI IWASA,⁶ TETSUYA TAKETSUGU,⁶ YORIKO
TOMINAGA,⁷ SAULIUS JUODKAZIS^{3,8}

¹Department of Physics, Electrical and Computer Engineering, Graduate School of Engineering, Yokohama National University, 79-5 Tokiwadai, Hodogaya-ku, Yokohama 240-8501, Japan.

²Department of Materials Science and Engineering, Graduate School of Engineering, Yokohama National University, 79-5 Tokiwadai, Hodogaya-ku, Yokohama 240-8501, Japan.

³Centre for Micro-Photonics, Faculty of Science, Engineering and Technology, Swinburne University of Technology, Hawthorn, VIC 3122, Australia

⁴Center for Physical Sciences and Technology, A. Goštauto 9, LT-01108 Vilnius, Lithuania.

⁵Paul Scherrer Institute, Villigen CH-5232, Switzerland

⁶Department of chemistry, Faculty of science, Hokkaido University, N10, W8, Kita-ku Sapporo, Hokkaido 060-0810 Japan.

⁷Graduate School of Advanced Sciences of Matter, Hiroshima University, 1-3-1, Kagamiyama, Higashihiroshima, Hiroshima 739-8530, Japan.

⁸Melbourne Center for Nanofabrication, Australian National Fabrication Facility, Clayton, VIC 3168, Melbourne, Australia.

*nishijima-yoshiaki-sp@ynu.ac.jp

Abstract: For hydrogen sensor and storage applications, films of Au and Pd were (i) co-sputtered at different rates or (ii) deposited in a sequential layer-by-layer fashion on a cover glass. Peculiarities of hydrogen uptake and release were optically monitored using 1.3 μm wavelength light. Increase of optical transmission was observed for hydrogenated Pd-rich films of 10-30 nm thickness. Up to a three times slower hydrogen release took place as compared with the hydrogen uptake. Compositional ratio of Au:Pd and thermal treatment of films provided control over the optical extinction changes and hydrogen uptake/release time constants. Higher uptake and release rates were observed in the annealed Au:Pd films as compared to those deposited at room temperature and were faster for the Au-richer films. Three main parameters relevant for sensors: sensitivity, selectivity, stability (reproducibility) are discussed together with the hydrogenation mechanism in Au:Pd alloys.

© 2018 Optical Society of America

OCIS codes: (160.4760) Optical properties; (310.6860) Thin films; (280.4788) Optical sensing and sensors; (240.6680) Surface plasmons; (160.3918) Metamaterials

References and links

1. S. K. Earl, T. D. James, T. J. Davis, J. C. McCallum, R. E. Marvel, R. F. Haglund, and A. Roberts "Tunable optical antennas enabled by the phase transition in vanadium dioxide," *Opt. Express* **21**, 27503-27508 (2013).
2. A. Baumel, P. Drodten, E. Heitz, and R. Bender, Chap. A 35. Platinum metals (Ir, Os, Pd, Rh, Ru) (John Wiley and Sons, 2008).
3. A. Tittl, C. Kremers, J. Dorfmueller, D. N. Chigrin, and H. Giessen, "Spectral shifts in optical nanoantenna-enhanced hydrogen sensors," *Opt. Mat. Express* **2**, 111-118 (2012).
4. C. Wadell, and C. Langhammer, "Drift-corrected nanoplasmonic hydrogen sensing by polarization," *Nanoscale* **7**, 10963-10969 (2015).
5. N. Strohfeldt, J. Zhao, A. Tittl, and H. Giessen, "Sensitivity engineering in direct contact palladium-gold nano-sandwich hydrogen sensors," *Opt. Mat. Express* **5**, 2525-2535 (2015).
6. N. S. Lewis, and D. G. Nocera, "Powering the planet: Chemical challenges in solar energy utilization," *Proc. Nat. Acad. Sci.* **103**, 15729-15735 (2006).

7. K. Juodkazis, J. Juodkazyte, P. Kalinauskas, E. Jelmakas, and S. Juodkazis, "Photoelectrolysis of water: Solar hydrogen-achievements and perspectives," *Opt. Express: energy express* **18**, A147-A160 (2010).
8. G. Gahleitner, "Hydrogen from renewable electricity: An international review of power-to-gas pilot plants for stationary applications," *Int. J. Hydrogen Energy* **38**, 2039-2061 (2013).
9. M. M. May, H. J. Lewerenz, D. Lackner, F. Dimroth, and T. Hannappel, "Efficient direct solar-to-hydrogen conversion by in situ interface transformation of a tandem structure," *Nature Commun.* **6**, 8286 1-7 (2015).
10. A. Nakamura, Y. Ota, K. Koike, Y. Hidaka, K. Nishioka, M. Sugiyama, K. Fujii, "A 24.4 solar to hydrogen energy conversion efficiency by combining concentrator photovoltaic modules and electrochemical cells," *Appl. Phys. Express* **8**, 107101 (2015).
11. A. D. Assl, D. E. Gomez, A. Roberts, and T. J. Davis, "Frequency-dependent optical steering from subwavelength plasmonic structures," *Opt. Lett.* **37**, 4206-4208 (2012).
12. J. I. Avila, R. J. Matelon, R. Trabol, M. Favre, D. Lederman, U. G. Volkmann, A. L. Cabrera, "Optical properties of Pd thin films exposed to hydrogen studied by transmittance and reflectance spectroscopy," *J. Appl. Phys.* **107**, 023504 (2010).
13. I. Aruna, B. R. Metha, and L. K. Malhotra, "Faster H recovery in Pd nanoparticle layer based Gd switchable mirrors: Size-induced geometric and electronic effects," *Appl. Phys. Lett.* **87**, 103101 1-3 (2005).
14. I. Aruna, B. R. Mehta, L. K. Malhotra, and S. M. Shivaprasad, "A color-neutral, Gd nanoparticle switchable mirror with improved optical contrast and response time," *Adv. Mater.* **16**, 169-173 (2004).
15. S. Tomonari, H. Yoshida, M. Kamakura, K. Yoshida, K. Kawahito, M. Saitoh, H. Kawada, S. Juodkazis, H. Misawa, "Efficient microvalve driven by a Si-Ni bimorph," *Jpn. J. Appl. Phys.* **42**, 4464-4468 (2003).
16. S. Tomonari, H. Yoshida, M. Kamakura, K. Yoshida, K. Kawahito, M. Saitoh, H. Kawada, S. Juodkazis, H. Misawa, "Miniaturization of a thermally driven Ni-Si bimorph," *Jpn. J. Appl. Phys.* **42**, 4593-4597 (2003).
17. Y. Nishijima, and S. Akiyama, "Unusual optical properties of the Au/Ag alloy at the matching mole fraction," *Opt. Mat. Express* **2**, 1226-1235 (2012).
18. C. Gong, and M. S. Leite, "Noble metal alloys for plasmonics," *ACS Photon.* **3**, 507-513 (2016).
19. C. Gong, M. Rebello, S. Dias, G. C. Wessler, J. A. Taillon, L. G. Salamanca-Riba, M. S. Leite, "Near-field optical properties of fully alloyed noble metal nanoparticles," *Adv. Opt. Mater.* **5**, 1600568, 1-6 (2017).
20. Y. Hashimoto, G. Seniutinas, A. Balcytis, S. Juodkazis, and Y. Nishijima, "Au-Ag-Cu nano-alloys: tailoring of permittivity," *Sci. Reports* **6**, 25010 1-9 (2016).
21. K. Kusada, M. Yamauchi, H. Kobayashi, H. Kitagawa, Y. Kubota, "Solid solution alloy nanoparticles of immiscible Pd and Ru elements neighboring on Rh: Changeover of the thermodynamic behavior for hydrogen storage and enhanced CO-oxidizing ability," *J. Am. Chem. Soc.* **136**, 1864-1871 (2014).
22. K. Kusada, M. Yamauchi, H. Kobayashi, H. Kitagawa, and Y. Kubota, "Hydrogen-storage properties of solid-solution alloys of immiscible neighboring elements with Pd," *J. Am. Chem. Soc.* **132**, 15896-15898 (2010).
23. M. Hirano, K. Enokida, K. Okazaki, S. Kuwabata, H. Yoshida and T. Torimoto "Composition-dependent electrocatalytic activity of AuPd alloy nanoparticles prepared via simultaneous sputter deposition into an ionic liquid," *Phys. Chem. Chem. Phys.* **15**, 7286-7294 (2013).
24. M. F. Juarez, G. Soldano, H. Guesimi, F. Tielens, and E. Santos, "Catalytic properties of Au electrodes modified by an underlayer of Pd," *Surf. Sci.* **631**, 235-247 (2015).
25. H. Kobayashi, K. Kusada, and H. Kitagawa, "Creation of novel solid-solution alloy nanoparticles on the basis of density-of-states engineering by interelement fusion," *ACC. Chem. Res.* **48**, 1551-1559, (2015).
26. M. Pourbaix, "Atlas of electrochemical equilibria in aqueous solutions" National Association of Corrosion Engineers, 1974.
27. J. P. Perdew, K. Burke, and M. Ernzerhof, "Generalized gradient approximation made simple," *Phys. Rev. Lett.* **77**, 3685, (1996).
28. P. E. Blochl, "Ab initio molecular dynamics for liquid metals," *Phys. Rev. B* **50**, 17953 (1994).
29. G. Kresse, and J. Hafner, "Ab initio molecular dynamics for liquid metals," *Phys. Rev. B* **47**, RC558 (1993).
30. G. Kresse, "Ab initio Molekular Dynamik fur flussige Metalle," Ph.D. thesis, Diss., Techn. Universitat Wien (1993).
31. G. Kresse, and J. Furthmuller, "Efficiency of ab-initio total energy calculations for metals and semiconductors using a plane-wave basis set," *Comput. Mat. Sci.* **6**, 1-50 (1996).
32. G. Kresse, and J. Furthmuller, "Efficient iterative schemes for ab initio total-energy calculations using a plane-wave basis set," *Phys. Rev. B* **54**, 11169 (1996).
33. S. Okazaki, and S. Johjima, "Temperature dependence and degradation of gasochromic responsebehavior in hydrogen sensing with Pt/WO₃ thin film," *Thin Solid Films* **558**, 411-415 (2014).
34. A. E. Bon and I. K. Kagan, "Stroyeniye i svoystva dvoynikh metalicheskikh sistem (in Russian)" (Nauka, Moscow, 1976).
35. X. Teng, Q. Wang, P. Liu, W. Han, A. I. Frenkel, W. Wen, N. Marinkovic, J. C. Hanson, J. A. Rodriguez, "Formation of Pd/Au nanostructures from Pd nanowires via galvanic replacement reaction," *J. Am. Chem. Soc.* **130**, 1093-1101 (2008).
36. M. Murakami, D. deFontaine, and J. Fodor, "X-ray diffraction study of interdiffusion in bimetallic Au/Pd thin films," *J. Appl. Phys.* **47**, 2850-2856 (1976).
37. H. Nakajima, H. Fujimori, and M. Koiwa, "Interdiffusion and structural relaxation in Mo/Si multilayer films," *J. Appl. Phys.*, **63**, 1046-1051 (1988).

38. I. K. Schuller, "New class of layered materials," *Phys. Rev. Lett.* **44**, 1597-1600 (1980).
39. B. M. Clemens, and J. G. Gay, "Effect of layer-thickness fluctuations on superlattice diffraction," *Phys. Rev. B* **35**, 9337-9340, (1987).
40. Y. Tominaga, Y. Kinoshita, K. Oe, and M. Yoshimoto, "Structural investigation of GaAs_{1-x}Bix/GaAsGaAs_{1-x}Bix/GaAs multi-quantum wells," *Appl. Phys. Lett.* **93**, 131915 (2008).
41. Z. Zhao, M. Carpenter, H. Xi, and D. Welch, "All-optical hydrogen sensor based on a high alloy content palladium thin film," *Sensors and Actuators B* **113**, 532-538 (2006).
42. Y. Nishijima, A. Balčytis, G. Seniutinas, S. Juodkazis, T. Arakawa, S. Okazaki, Raimondas Petruškevičius, "Plasmonic Hydrogen Sensor at Infrared Wavelength," submitted, (2017).
43. A. Tittl, P. Mai, R. Taubert, D. Dregely, N. Liu, and H. Giessen, "Palladium-based plasmonic perfect absorber in the visible wavelength range and its application to hydrogen sensing," *Nano Lett.*, **11**, 4366-4369, (2011).
44. K. Juodkazis, J. Juodkazyte, B. Sebek, and S. Juodkazis, "Reversible hydrogen evolution and oxidation on Pt electrode mediated by molecular ion," *Appl. Surf. Sci.* **290**, 13-17 (2014).
45. K. Juodkazis, J. Juodkazyte, A. Griguševičienė and S. Juodkazis, "Hydrogen species within the metals: role of molecular hydrogen ion H₂," *Appl. Surf. Sci.* **258**, 743-747 (2011).
46. I. Wei, and J. Brewer, "Desorption of hydrogen from palladium plating," *AMP J. Technol.* **5**, 49-53 (1996).
47. S. Zhao, Z. Z. Tian, J. N. Liu, Y. L. Ren, and J. J. Wang, "Interaction of H₂ with gold-palladium binary clusters: Molecular and dissociative adsorption," *Computat. Theor. Chem.* **1055**, 1-7 (2015).
48. R. M. Holmes, "The effect of absorbed hydrogen on the thermoelectric properties of palladium," *Science* **LVI**, 201-202 (1922).
49. D. A. Otterson, and R. J. Smith, "Absorption of hydrogen by palladium and electrical resistivity up to H-Pd atom ratios of 0.97," NASA report, National Aeronautics and Space Administration, Washington DC (1969).
50. L. Pauling, "The nature of the chemical bond. iv. the energy of single bonds and the relative electronegativity of atoms," *J. Am. Chem. Soc.* **54**, 3570-3582 (1932).
51. D. Monzon-Hernandez, D. Luna-Moreno, and D. Martinez-Escobar, D. "Fast response fiber optic hydrogen sensor based on palladium and gold," *Sens. Actuators B: Chem.* **136**, 562-566 (2009).
52. L. Holleck, "Diffusion and solubility of hydrogen in palladium and palladium-silver alloys," *J. Phys. Chem.* **74**, 503-511, (1970).
53. W. Y. Yu, G. M. Mullen, and C. B. Mullins, "Hydrogen adsorption and absorption with Pd-Au bimetallic surfaces," *J. Phys. Chem. C* **117**, 19535-19543 (2013).
54. P. M. Quaino, R. Nazmutdinov, L. F. Peiretti, and E. Santos, "Unravelling the hydrogen absorption process in Pd overlayers on a Au(111) surface," *Phys. Chem. Chem. Phys.* **18**, 3659-3668 (2016).

1. Introduction

Plasmonic applications are expanding into a wider spectral range from UV to THz by harnessing peculiarities of dielectric permittivity, $\tilde{\epsilon}$, in different materials at the wavelengths of interest. Strong changes of the real and imaginary parts of the permittivity occur as a result of phase transitions, phase intermixing or chemical reactions [1]. For example, the affinity of Pd to hydrogen, which can be absorbed with an anomalously high volume ratio of ~ 600 for solid Pd [2], alters the optical response of Pd via changes in effective permittivity [3–5]. For future solar hydrogen applications and in fuel cells [6–9], storage and monitoring of hydrogen is of paramount importance. Hence, sensing capabilities have to keep pace with the rapid development in solar-to-hydrogen conversion, which in current state of the art industrial installation has reached 24.4% [10].

Detection of hydrogen using non-contact optical readout was demonstrated by orientational optical plasmonic scattering [11] and spectral shifts in polarization sensitive extinction [3, 4]. However, a more sensitive optical detection of Pd hydrogenation can be obtained by transmission measurements [12]. A "switchable mirror" that have a rare metal (Gd or Y) mirror with Pd thin film on top shows a large transmission change in visible wavelength region [13, 14]. Such sensors can provide a highly desirable non-contact method of hydrogen sensing and monitoring, especially in micro-chip applications where standard electrical resistance measurement is not desirable due to feasibility of a dielectric breakdown/discharge [15, 16].

Despite the exceptional affinity of Pd towards hydrogen other important parameters, such as response times and stability should ideally be fine-tuned for specific applications. The primary way of controlling the properties of metals is through creation of alloys. Permittivity control by co-sputtering of Ag and Au has been demonstrated to provide a possibility to engineer the

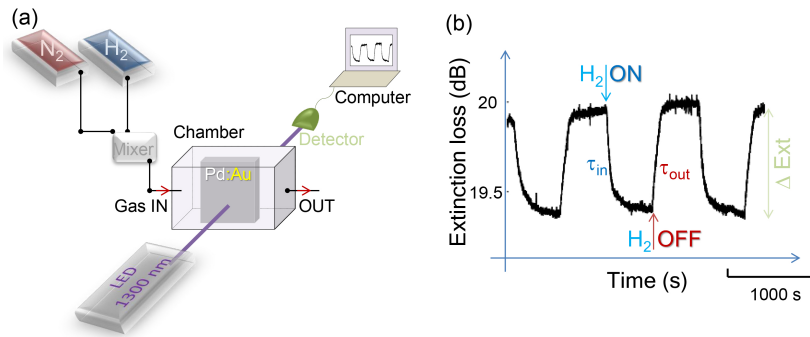


Fig. 1. (a) Setup for measurement of hydrogenation. (b) Extinction losses $Ext \equiv -10 \lg(I_t/I_0)$ [dB] where $I_{t,0}$ are the transmitted and reference intensities, respectively. Hydrogenated Pd becomes more transparent. ΔExt is the change of extinction losses between hydrogen saturated and depleted states.

optical response of a binary alloy [17–19] and was recently extended to ternary Au, Ag and Cu alloys [20]. Solid solutions of Rh and Ag mixed at the atomic level can store hydrogen much like Pd, a functionality non-existent either in pure Rh or Ag [21]. Another development of great interest is that Pd and Ru alloy nano-crystals enable CO oxidation catalysis superior to that of Rh [22]. Also, Au and Pd alloy nanoparticles enhance electrocatalytic activities [23]. Alloys tailored at the nanoscale are expected to bring forward new functionalities due to particular geometric configuration of atoms and strain resulting from the mismatch of lattice constants [24], as well as due to different electron binding and charge distribution which alters their chemical behavior [25].

Here, we prepare films of Au and Pd at different alloy intermixing ratios for prospective applications in hydrogen detection and storage. Optical readout of transmittance changes during hydrogen uptake and release was monitored using a simple non-contact method. Thereby the effect of alloy composition as well as alloying conditions on sensitivity to ambient hydrogen was elucidated. Detailed understanding of basic reactions with hydrogen are important for designing optical hydrogen sensor devices.

2. Samples and Methods

A series of Au and Pd intermixed samples were prepared by magnetron sputtering (Axxis, JKLesker) using two modes of deposition: (i) co-sputtering (Au:Pd) and (ii) alternating Au and Pd layers (Au-Pd) with different thicknesses deposited onto a 0.4-mm-thick cover glass. In the latter case, the numbers of alternation cycles were: 2, 4, 10, 20 (a pair of Au and Pd layers per one cycle) with corresponding effective thicknesses of 7.50, 3.75, 1.50, 0.75 nm/cycle, respectively. Sputtering rate was calibrated using the optical interference microscope 3D profiler (Bruker Co. Ltd.). Also the thickness of multi-layered samples were analyzed using X-ray diffraction (XRD). During sputtering, the substrate was either kept at room temperature or heated at 250°C. At normal conditions, Pd has its native surface [26].

The density of states (DOS) for Au, Pd, and AuPd alloys are calculated at the structures optimized using the Perdew-Burke-Ernzerhof generalized gradient approximation (PBE) [27] and the projector augmented wave method [28] as implemented in the VASP code [29–32]. The Au-Pd alloys are constructed by alternating Au and Pd layers in a 2-by-2 manner in the $\langle 001 \rangle$ direction using the unit cell consisting of Au_4Pd_4 and 1-by-2 in the $\langle 111 \rangle$ direction, using the unit cell consisting of $AuPd_2$. For both types of alloy systems, a $21 \times 21 \times 11$ k -point mesh is

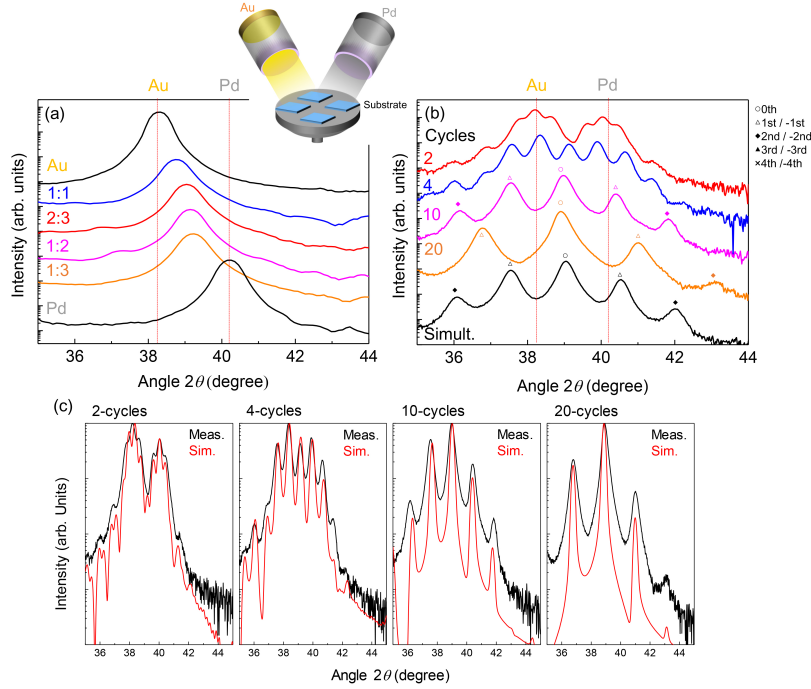


Fig. 2. (a) XRD of Au:Pd films co-sputtered onto a 250°C pre-heated glass substrate at different sputtering rates. Vertical lines mark (111) position of the fcc-Au and Pd peaks. (b) XRD of layered Au:Pd films in the range 40 to 70 nm thickness deposited at alternating cycles: 2, 4, 10, 20 (corresponding thicknesses are 7.50, 3.75, 1.50, 0.75 nm, respectively) and simultaneously deposited. (c) The experimentally measured XRD spectra (Meas.) and simulation (Sim.) results of alternating sputtering

used with the cutoff energy of 500 eV.

Optical permittivity of the samples was determined by transmission and reflection measurements using setup and analysis method reported earlier [20] at normal incidence. For hydrogenation of samples, all the optical setup was put into a sealed container with dimensions 50×50×15 cm³. The spectral range from 450 to 1000 nm was used as defined by limits of the used detectors.

Due to the flow rate limitation, the time dependence of hydrogen uptake was measured using a setup (Fig. 1) with a 21.4 cm³ sample chamber equipped with a gas mixing system to provide 500 mL/hour flow rate of a 4% H₂:N₂ mixture at a pressure of 0.1 MPa (~ 1 bar), a 1.31 μm wavelength laser emitting diode (ILX lightwave Co. MPS- 8012) and a Ge photo diode detector (Ando Electric Co., Ltd., AQ2150A) was used to *in situ* monitor transmission changes. A fiber optic collimator/focuser with a numerical aperture $NA = 0.25$ (Edmund Optics, Ltd.) was used to define the 2-mm-diameter spot on the metal film inside the gas chamber [33]. The used wavelength is out of the range used for the permittivity measurements. However for the most of metals, permittivity can be approximated by the Drude-Lorentz theory. Therefore behavior at 1.31 μm can be extrapolated from the results obtained in the visible spectral range following generic dependence:

$$\varepsilon(\omega) = \varepsilon(\infty) - \frac{\omega_p^2}{\omega^2 + i\omega/\tau} + \sum_j \frac{A_j \hbar\omega_{0,j}}{(\hbar\omega_{0,j})^2 - (\hbar\omega)^2 - i\hbar\omega/\tau_j}, \quad (1)$$

where the first two terms represent the Drude free electron model and the last term is the Lorentz

contribution accounting for the bound electrons participating in interband transitions. Here $\varepsilon(\infty)$ is the permittivity at the high frequency limit (infinity), ω_p is the plasma frequency, τ is the relaxation time of the free electrons; j denotes the index of a Lorentz oscillator, A_j , $\omega_{0,j}$ and τ_j are the amplitude, the resonant frequency and the relaxation time of the given oscillator j , respectively, \hbar is the reduced Plank constant, i is the imaginary unit, and ω is the optical cyclic frequency.

3. Results and discussion

3.1. Au:Pd alloy formation during sputtering

For hydrogen uptake and storage investigations, films of Au and Pd were prepared on a cover glass by co-sputtering both Au and Pd metals at different rates or by using layer-by-layer alternating sputtering. Pd and Au are known to be completely miscible to form solid solutions [24, 34]. Coatings of different thicknesses were deposited at room temperature (RT) or at 250°C substrate temperatures. Structure of the films was inspected using XRD and showed a continuous intermixing of Au and Pd in the case of films co-sputtered onto a 250°C heated substrate at different sputtering rates (Fig. 2(a)). A continuous shift of the $\langle 111 \rangle$ peak without a significant change of its width is indicative of well controlled alloying of Au and Pd and was better than was obtained by chemical exchange reactions on colloidal nanoparticles [35]. On the other hand, for Au-Pd films made by alternating sputtering of Au and Pd a complex XRD pattern was observed. This reflects a nano-cluster structure, since the constituent 2-3 nm thickness films (as judged by sputtering time) do not result in a continuous fully intermixed material (Fig. 2(b)).

Alloying of Au and Pd was previously studied as a diffusion constant, D , dependent process [36]. The intermixing rate was governed by D values of $\sim 10^{-10} \text{cm}^2/\text{s}$ at 1000°C and $D \sim 10^{-15} \text{cm}^2/\text{s}$ at 350°C. At the lower temperature of 250°C, the expected values of D range from 10^{-16} to $10^{-17} \text{cm}^2/\text{s}$, and are even more significantly diminished at RT. Therefore, appreciable migration of atoms is not expected at RT.

By alternating sputtering, multi layers of Au and Pd were formed as observed by XRD. The samples made by 2 and 4 cycles of sputtering showed characteristic separate Au and Pd XRD profiles which were not forming a periodic layered structure. However, in the case of 10 and 20 cycles, the pure Au and Pd profiles have disappeared and satellite peaks in XRD identified formation of layered structure.

The multiple satellite peaks are well known in the field of semiconductor super-lattice materials with similar XRD profiles [37–40]. From the satellite peaks, it is possible to calculate the thickness of each layer by using the Bragg equation:

$$\Lambda = \frac{m - n}{\sin \theta_m - \sin \theta_n} \frac{\lambda}{2}, \quad (2)$$

where $\lambda = 0.15148 \text{ nm}$ is the characteristic X-ray wavelength of the Cu K_α line. The suffixes m or n respectively define the m -th or n -th peak orders at the XRD spectra. The diffraction multi-peaks were analyzed using a simulation program LEPTOS, Bruker AXS, which is based on the dynamical theory of diffraction (see Fig.2 (c)). Such analysis, provides possibility to cross check results of numerical calculations with XRD experimental data. A single layer thicknesses Λ was deduced to be 20 nm (for 2 cycles), 12 nm (4 cycles), 6.4 nm (10 cycles), and 3.4 nm (20 cycles), respectively. Total thickness of the film has been estimated to range from 40 to 68 nm.

Similar satellite XRD peaks to those resulting from alternating deposition were likewise observed for Pd:Au films co-sputtered onto a RT substrate. The origin of those satellite peaks in the case of simultaneous co-sputtering needs more detailed analysis. However, qualitatively they can be explained by the relative position of the rotating substrate stage in relation to the sputtering sources. As the substrate plane is tilted with respect to both of the sources, a gradient of deposition rates develops along the diameter of the sample [18]. So, as the substrate rotates during

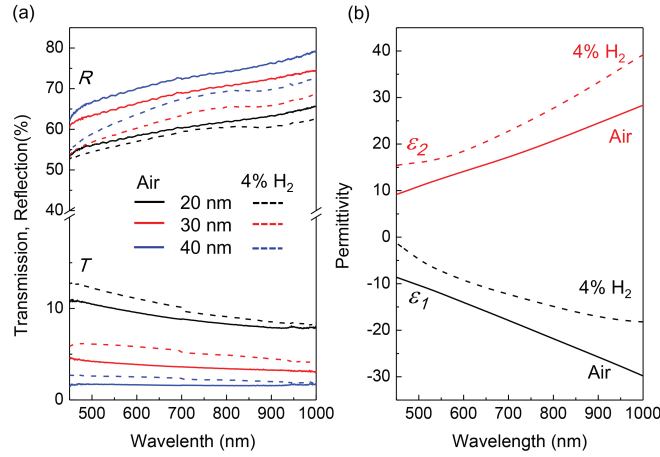


Fig. 3. (a) Optical transmission and reflection of Pd thin films (thickness 20, 30 40 nm) with 4% H₂ or N₂ (without H₂) condition, and (b) optical permittivity of the Pd with/without H₂

sputtering, periodic oscillations in alloy composition emerge and, at RT, diffusion proceeds too slowly to efface them. The films prepared by sputtering, each with different structural properties, was tested next for their hydrogen uptake and release capability.

3.2. Hydrogen storage and optical properties of metals

Hydrogen storage has to be both reversible and rapid for practical applications [41]. The interaction between Pd and H affects their optical properties. Figure 3 shows optical spectroscopic change occurred due to a hydrogen uptake. Typically, transmittance increased while reflectance decreased. An optical transmission measurement of a Pd film hydrogenation is sensitive due to the exponential dependence of transmittance, T , on the imaginary part of the refractive index of a strongly absorbing film (Pd with hydrogen) $\tilde{n} = n + ik$ on a non-absorbing substrate of refractive index, n_s (glass) [12]:

$$T \simeq \frac{16n_s(n^2 + k^2)}{[(n + n_s)^2 + k^2][(1 + n)^2 + k^2]} e^{-\frac{4\pi kd}{\lambda}}, R \simeq \frac{(1 - n)^2 + k^2}{(1 + n)^2 + k^2} \quad (3)$$

where d is the thickness of the Pd film and λ is the wavelength of light. With these results, applying the Drude-Lorenz model, the real and imaginary part of the permittivity can be determined in the measured wavelength range. The Drude part, which consists of the ω_p and τ give us the important information for the free electron behavior. Where ω_p is the ratio of free carrier density and effective mass. τ is the relaxation time, which indicate the information of the electron scattering by the electron, hole, grain boundaries and the other scattering sources. When the hydrogen was absorbed into the Pd, the ω_p slightly increased from $1.5 \times 10^{16} \text{ s}^{-1}$ to $1.9 \times 10^{16} \text{ s}^{-1}$, τ decreased from $4.3 \times 10^{-16} \text{ s}$ to $3.0 \times 10^{-16} \text{ s}$. These optical parameter change would be related to the resonance wavelenth shift of the plasmon materials [17, 42, 43].

This increase of ω_p means the an increase of the free electron density and/or decrease of an effective mass of electron. Hydrogen might donate a free electron to the Pd or softened the bonding as discussed below. The decreasing τ is caused by the increasing of scattering inside the solid phase. The internally trapped hydrogen causes the scattering of electrons, therefore, the faster relaxation of free electron oscillation is obtained.

The absorbed hydrogen causes the binding between Pd and hydrogen tentatively describe as

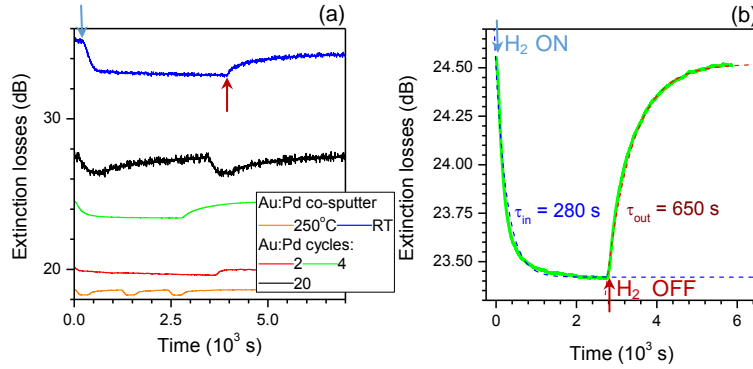


Fig. 4. Layers of Au-Pd made by alternating deposition. (a) Extinction [dB] changes during ON/OFF cycling of H₂ flow (marked by arrows) in the case of differently prepared Au-Pd layers at different mixing ratios deposited on RT or 250°C glass substrates; layers of Au and Pd were sputtered individually in cycles of 2, 4, 20 with total layer thickness in the range 40 to 70 nm. (b) Transient of the Au-Pd 4-cycle sample fitted with single exponential uptake and release time constants $\tau_{in,out}$, respectively.

PdH_x. Based on thermodynamic arguments there is a possibility of H⁺ or H₂⁺ species inside the metal [44, 45]. Earlier studies showed that upon hydrogenation of Pd there is heat generation, while for H₂ release an elevated temperature of > 150°C is required [46]. It is noteworthy that recent density functional calculations [47] of H₂ interaction with Au:Pd binary clusters revealed that H₂ molecules donate electrons to metal clusters in molecular adsorption. Hydrogen enters the interior of Pd with a larger inner surface area. Similar to the longevity of fuel cells, batteries, and super-capacitors, the reversibility of processes at the microscopic level during charging-discharging are critically important. In this case, the hydrogen uptake - release.

From the thermoelectric power experiment, hydrogen uptake causes an increase of electron density in the Pd host. However, the electrical resistivity is known to increase upon hydrogen uptake and, at room temperature, can be almost doubled at full hydrogenation, which depends on pressure [48, 49]:

$$\frac{H}{Pd} = 0.69 + \frac{\ln p_H/p_0}{36.8}, \quad (4)$$

where $\frac{H}{Pd}$ is the atomic ratio of H and Pd, p_H [bar] is the hydrogen pressure, and p_0 is the total pressure of the gas mixture. The electrons and hydrogen cations in Pd create an interesting guest-host system with an amazingly high ratio of $\frac{H}{Pd} \approx 0.95$ at high 16.5×10^3 bar pressure [49]; $\frac{H}{Pd} = 0.69$ at a hydrogen pressure equal to 1 bar (at normal conditions).

The results of this study on the optical response of the hydrogen uptake/release agree well with electrical response.

For hydrogen release from the solid Pd phase, a dramatic increase in size occurs from protons to H₂ directly or via an intermediate H₂⁺. This causes a steric hindrance for hydrogen release at the surface of Pd and, consequently, it takes longer. It is noteworthy, that the (bulk[⊖]|⊕gas) electron-ion pair mechanism is fully reversible, hence, is promising for practical storage applications where reversibility is the key requirement.

Optical readout of hydrogenation

A simple flow chamber with 4% H₂ in a N₂ carrier gas was set up with the possibility to monitor optical transmission changes upon hydrogenation of Au and Pd films at $\lambda = 1.31 \mu\text{m}$ wavelength (Fig. 1). Extinction losses were determined by measuring optical transmission:

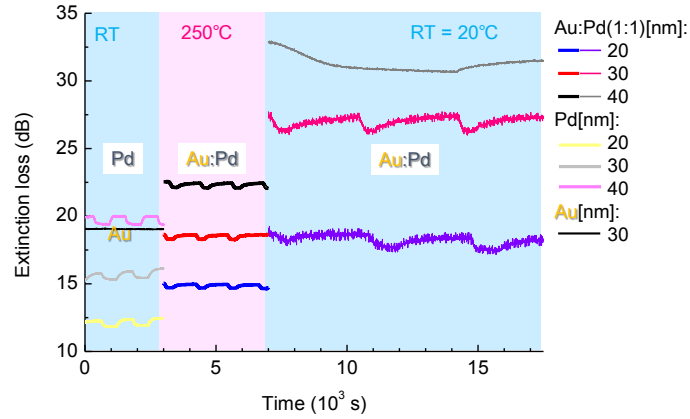


Fig. 5. Layer of Au:Pd made by co-sputtering. (a) Extinction losses, Ext , (Fig. 1(b)) during hydrogenation of pure Pd and Au:Pd (1:1) co-sputtered films of different thickness on pre-heated 250°C and RT glass substrates. For Au, $Ext = Const$ and not dependent on H_2 presence (horizontal line for Au of 20 nm).

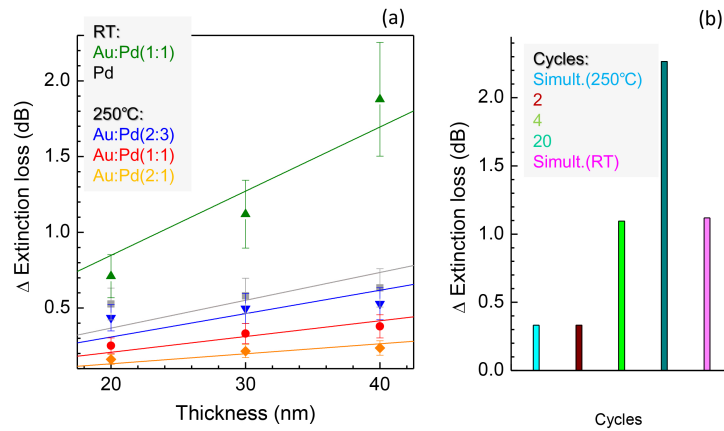


Fig. 6. (a) Change of extinction, ΔExt , for simultaneously co-sputtered films. Error bars are $\pm 20\%$ and the lines are guides for eye with starting point at origin of coordinates (0;0). (b) ΔExt for Au:Pd (1:1) multi layered and simultaneous sputtering (250°C and RT).

$Ext \equiv -10 \lg(I_t/I_0)$ [dB] where I_t, I_0 respectively are the transmitted and reference intensities; reference intensity $I_0 = 12.2 \mu W$ was measured without the sample in a N_2 filled chamber. Following the introduction of H_2 no measurable change in optical transmission was observed for pure Au films with thickness in the range of 10-30 nm. In the case of Pd containing films the presence of H_2 induced an increase in their transmittance. Figure 5 shows the total extinction of pure Pd as well as alloyed Au:Pd films and Ext changes as H_2 flow was cycled through the chamber. Of note is that the trend of decreased extinction with progressive hydrogenation enables increased precision of the measurement due to a better signal-to-noise ratio as more hydrogen is absorbed by Pd and a larger change in the extinction, ΔExt , is measured. Temporal evolution of hydrogen uptake and release were well fitted by single exponential transients (Eqn. 3) with time constants $\tau_{in,out}$, respectively (Fig. 1(b)). For the Au:Pd film, there was an obvious asymmetry

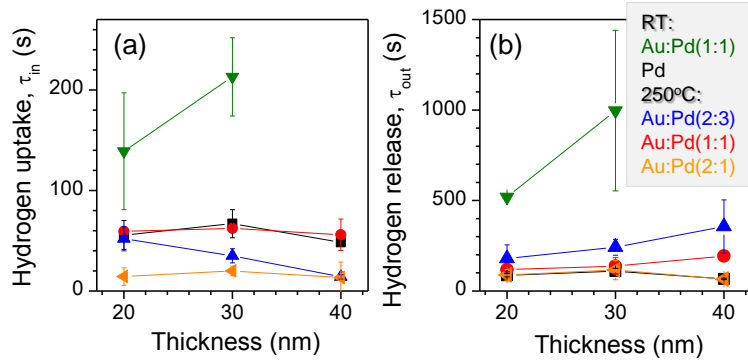


Fig. 7. Hydrogen uptake (a) and release (b) time constants $\tau_{in,out}$, respectively, for Au:Pd films prepared by co-sputtering with and without annealing.

$\tau_{in} < \tau_{out}$ (Fig. 5).

Films of Pd and Au:Pd sputtered onto a pre-heated substrate showed smaller optical losses in transmission, presumably due to a better homogeneity and smaller nano-porosity, as tested for several different thicknesses (Fig 5). Figure 6 shows the change of extinction losses due to hydrogenation (an increase in transmission) for differently prepared samples. Extinction [dB] was linearly dependent on thickness of Pd as one would expect from optical absorption. Interestingly, mixture Au:Pd (1:1) sputtered on substrate at RT showed the largest changes of extinction (Fig. 6(a)), even larger than in the case of pure Pd. When deposition of Pd and Au layers was carried out on a pre-heated substrate, smaller ΔExt values were observed (Fig. 6(b)). This could also be attributed to a greater extent of alloy lattice ordering in the case of alloy formation on a pre-heated substrate. The value of ΔExt was found to scale in proportion to the amount of Pd in the intermixed films.

The largest ΔExt observed in Au:Pd (1:1) alloy deposited on a RT substrate, had the slowest H_2 uptake time, τ_{in} (Fig 7(a)), markedly slower than in the pure Pd film [35]. In general, the presence of Au in the film decreased τ_{in} , most probably, due to a larger electro negativity of Au (2.54) as compared with Pd (2.22; same as H) according to the Pauling scale [50]. Hydrogen release time, τ_{out} , was approximately 2-3 times longer compared to the hydrogen uptake time (Fig 7(b)). A similar result was reported in ref. [51], where stacked Pd and Au nano-layers were deposited by thermal evaporation onto optical fibers and attenuation changes in evanescent wave upon hydrogenation of a multi-layered film were measured.

Surface adsorption / desorption on Au-Pd alloy

The hydrogen read out was found to be strongly influenced by Au:Pd alloying. The hydrogen diffusion constant D in Pd is on the order of 10^{-5} cm²/s [52]. Therefore, the diffusion time in a thin 10 nm film could be estimated at the order of $\sim 10\mu s$. This is much more rapid than observed in experiments. The rate limiting reaction is adsorption/desorption of hydrogen on the surfaces of metal thin films. Mullins et al. revealed that temperature defined the hydrogen desorption rate. A lower temperature desorption has been observed on the surface of Au:Pd alloying site. This indicated that alloying Au and Pd resulted in a decrease of affinity to hydrogen [53]. This effect can be also explained by the density of state (DOS) changes in Au and Pd alloy. Quaino et al. showed by density functional theory (DFT) calculations for Au(111) surface on Pd, that the Fermi level of an alloy was lower in energy due to the Au:Pd bond formation [54]. We have also confirmed this prediction by DFT calculations in Fig. 8. Hence, an alloy of Au:Pd would have a reduced activation energy for hydrogen adsorption and desorption on the surface. Therefore we

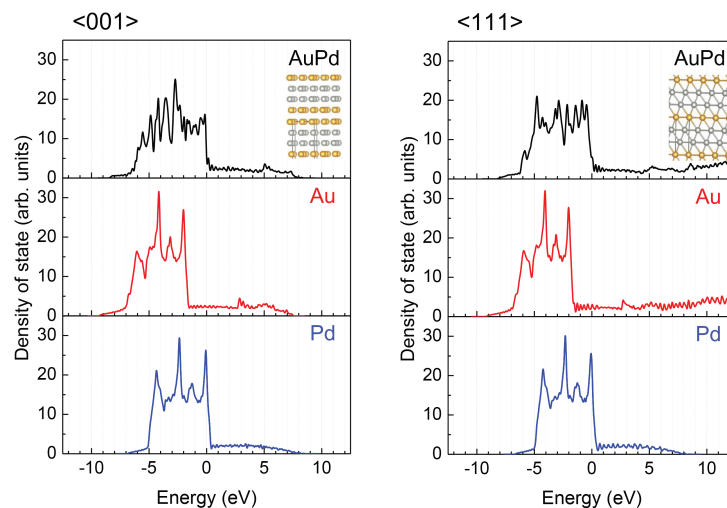


Fig. 8. The density of state (DOS) for AuPd alloy and pure Au, and Pd systems for the $\langle 001 \rangle$ (left column) and $\langle 111 \rangle$ (right column) orientations. Gold and silver spheres show Au and Pd, respectively. Zero in the energy x axis indicates the top of the occupied valence band.

have obtained faster uptake and release times in Au:Pd alloy films especially with annealed and homogeneously alloyed samples.

Conclusions

The mixture of Au and Pd made by co-sputtering can improve (shorten) the response time during H_2 uptake and release stages, most probably, due to electro negativity of Au which facilitates the adsorption of positively charged hydrogen species H_2^+ and H^+ at the inner surface of the alloy phase. Multi-layered sample made by alternating sputtering has higher sensitivity as compared with co-sputtered samples. Stability in H_2 uptake-release performance showed no difference on a day-to-day basis. This is consistent with earlier observations that embitterment during hydrogenation can be avoided [46]. The fully reversible mechanism of hydrogen uptake into Pd phase is promising for applications where long term stability is of paramount importance. Using Au:Pd mixtures it is possible to enable more rapid and sensitive optical hydrogen monitoring device construction.

Acknowledgement

YN grateful for partial support by Japan Society for the Promotion of Science (JSPS), Grants-in-Aid for Scientific Research, Open Partnership Joint Projects of JSPS Bilateral Joint Research Projects and Tateishi foundation. Amada foundation. SJ acknowledges a partial support via the Australian Research Council Discovery project DP130101205 and a startup funding of Nanotechnology facility by Swinburne University. The computation in this work has partly been done using the facilities of the Supercomputer Center, the Institute for Solid State Physics, the University of Tokyo. Authors greatly thank to Dr. Hitoshi Morioka of Bruker AXS K.K., and Professor Masahiro Yoshimoto and Assistant Professor Hiroyuki Nishinaka of Kyoto Institute of Technology for their helps with the simulation analysis of XRD spectra.